Unsupervised Classification of Atrial Electrograms for Electroanatomic Mapping of Human Persistent Atrial Fibrillation

Tiago P. Almeida, *Member, IEEE*, Diogo C. Soriano, Michela Masè, Flavia Ravelli, Arthur S. Bezerra, Xin Li, Gavin S. Chu, João Salinet, Peter J. Stafford, G. André Ng, Fernando S. Schlindwein, *Member, IEEE*, and Takashi Yoneyama

Abstract*—*Objective: **Ablation treatment for persistent atrial fibrillation (persAF) remains challenging due to the absence of a 'ground truth' for atrial substrate characterization and the presence of multiple mechanisms driving the arrhythmia. We implemented an unsupervised classification to identify clusters of atrial electrograms (AEGs) with similar patterns, which were then validated by AEG-derived markers.** ***Methods*****: 956 bipolar AEGs were collected from 11 persAF patients. CARTO variables (Biosense Webster; ICL, ACI and SCI) were used to create a 3D space, and subsequently used to perform an unsupervised classification with k-means. The characteristics of the identified groups were investigated using nine AEG-derived markers: sample entropy (SampEn), dominant frequency, organization index (OI), determinism, laminarity, recurrence rate (RR), peak-to-peak (PP) amplitude, cycle length (CL), and wave similarity (WS).** ***Results*****: Five AEG classes with distinct characteristics were identified ($F = 582$, $P<0.0001$). The presence of fractionation increased from class 1 to 5, as reflected by the nine markers. Class 1 (25%) included organized AEGs with high WS, determinism, laminarity, and RR, and low SampEn. Class 5 (20%) comprised fractionated AEGs with in low WS, OI, determinism, laminarity, and RR, and in high SampEn. Classes 2 (12%), 3 (13%) and 4 (30%) suggested different degrees of AEG organization.** ***Conclusions*****: Our results expand and reinterpret the criteria used for automated AEG classification. The nine markers highlighted electrophysiological differences among the five classes found by the k-means, which could provide a more complete characterization of persAF substrate during ablation target identification in future clinical studies.**

***Index Terms*—Atrial fibrillation, catheter ablation, electrophysiology mapping, unsupervised classification, k-means.**

Manuscript received April 3, 2020; revised July 18, 2020 and August 28, 2020; accepted August 29, 2020. Date of publication September 3, 2020; date of current version March 19, 2021. This work was supported in part by the NIHR Leicester Biomedical Research Centre, in part by the FAPESP (Brazil, 2015/12799-9, 2017/00319-8, 2018/02251-4 and 2019/05192-1), in part by the BHF (PG/18/33/33780 and Research Accelerator for ECR), in part by the CNPq (Brazil, 200598/2009-0, 449467/2014-7 and 305616/2016-1), in part by the Fondazione Cassa di Risparmio di Trento e Rovereto (2016.0273) and in part by the MRC UK (DPFS MR/S037306/1). *(Corresponding author: Tiago P. Almeida.)*

Tiago P. Almeida is with the Department of Cardiovascular Sciences, University of Leicester, Glenfield Hospital, Leicester LE3 9QP, U.K., with the School of Engineering, University of Leicester, Leicester LE1 7RH, U.K., and also with the Aeronautics Institute of Technology, São José dos Campos, São Paulo 12228-900, Brazil (e-mail: tpda2@le.ac.uk).

Diogo C. Soriano and João Salinet are with the Federal University of ABC.

Michela Masè is with the Università degli Studi di Trento with the IRCS-HTA, Healthcare Research and Innovation Program, Bruno Kessler Foundation.FBK, and also with the Institute of Mountain Emergency Medicine, Eurac Research.

Flavia Ravelli is with the Università degli Studi di Trento.

Arthur S. Bezerra is with the Aeronautics Institute of Technology.

Xin Li is with the Department of Cardiovascular Sciences, University of Leicester and also with the School of Engineering, University of Leicester.

Gavin S. Chu is with the Department of Cardiovascular Sciences, University of Leicester and also with the University Hospitals of Leicester NHS Trust.

Peter J. Stafford is with the University Hospitals of Leicester NHS Trust.

G. André Ng is with the Department of Cardiovascular Sciences, University of Leicester, with the University Hospitals of Leicester NHS Trust, and also with the National Institute for Health Research Leicester Cardiovascular Biomedical Research Centre, Glenfield Hospital.

Fernando S. Schlindwein is with the School of Engineering, University of Leicester and also with the National Institute for Health Research Leicester Cardiovascular Biomedical Research Centre, Glenfield Hospital.

Takashi Yoneyama is with the Aeronautics Institute of Technology.

This article has supplementary downloadable material available at https://ieeexplore.ieee.org, provided by the authors.

Digital Object Identifier 10.1109/TBME.2020.3021480

I. Introduction

MILLIONS of patients suffer from atrial fibrillation (AF), the most common sustained arrhythmia in clinical practice. AF is characterized by the uncoordinated activation of the atria and is a leading cause of hospitalization and cardiovascular complications, particularly stroke [1].

Catheter ablation is established as a good percutaneous therapy for drug refractory AF [1]. Pulmonary vein isolation (PVI) is considered a cornerstone for AF ablative therapy, especially in the early stages of the disease [1], [2]. For persistent AF (persAF), however, the ablation outcomes remain suboptimal, and it is still not clear where to apply ablation lesions in order to stop AF and prevent its recurrence. That is because sustained AF causes changes in cardiac tissue, inducing structural and electrical remodeling [1]. The presence of remodeled tissue can produce slow or inhomogeneous conduction, inducing reentry circuits, resulting in fractionated fibrillatory conduction—important in triggering and perpetuating the arrhythmia [3].

Multiple mechanisms have been linked to persAF perpetuation, such as rapidly discharging automatic foci [2]; multiple

wavelets [4]; single reentrant circuits with fibrillatory conduction [5]; functional reentry resulting from rotors [6]; and epi-endocardial conduction dissociation [7]. These mechanisms may co-exist either simultaneously or intermittently, manifesting differently in each patient [8]. Therefore, ablation strategies have been proposed to guide ablation tailored to patient-specific pathophysiology [8]. As such, biomarkers derived from intracardiac atrial electrograms (AEGs) collected during persAF have been used to characterize patient-specific atrial substrate to guide ablation—*e.g.*, AEG fractionation to target anisotropic conduction [3]; phase analysis to locate rotors [6]; AEG amplitude to ablate fibrotic tissue [9]; and the dominant frequency (DF) of AEGs to target rapidly discharging automatic foci [10]. Several of these markers have been embedded in commercial electroanatomic mapping (EAM) systems to help the operator design the ablation strategy based on the operator's experience, culminating in a dichotomized decision of whether or not ablate the mapped atrial regions [11]. Each of the solutions embedded in EAM systems are specific for a single distinct pathomechanism—*e.g.*, AEG fractionation, rotors, ectopic beats etc. Therefore, each system provides a map with a range of values for a marker based on the specific pathomechanism that can be used as an auxiliary tool for therapy planning and strategy for ablation. The systems allow for different thresholds for the marker, depending on the cardiologist's experience [11]. Although this helps tailoring the ablation strategy based on one specific pathomechanism, the presence of multiple AF sources and mechanisms as well as the subjectivity in defining thresholds for the markers might hinder ablation target identification based on such marker. As a result, ablation outcomes have been shown inconsistent, and current solutions have failed to provide a definitive answer for persAF therapy [12], [13]. Novel methods that investigate markers to improve automated identification of targets for ablation need to be devised [8], [14].

The nature of this problem— data without defined categories or classes, in this case represented by the lack of a 'ground truth' for the atrial substrate—motivates the investigation of unsupervised methods that estimate possible classes of AF AEGs through the combination of markers. This approach may help unveil previously undetected electrophysiologic (EP) characteristics [15]. The resulting classification needs extensive investigation to interpret the discovered classes and relate them with EP phenomena. Few studies conducted unsupervised clustering in cardiac signals, most of them using non-invasive cardiac signals [16]. For instance, a self-organizing map (SOM) technique was applied in ECGs for the automated clustering of different types of QRS complexes, which resulted in more than fifteen types of heartbeats—including irregular atrial activity [17]. Expectation maximization from compressed ECG has been used for the diagnosis of cardiovascular abnormalities including AF, with 97% overall accuracy [18]. Cluster analysis performed on selected features extracted from ECGs was effective in discriminating sinus rhythm from a group of abnormal heartbeats, including left bundle branch block, right bundle branch block, premature ventricular contractions and atrial premature contractions [19]. Recently, Donosan and colleagues performed clustering based on three features extracted from the ECGs: the peak frequency mean value, peak frequency standard deviation and the spectral concentration [20]. Their results suggest the existence of five different types of ECGs during AF. In intracardiac signals, different classes/types of activations were identified in single AEGs during AF using principal component analysis (PCA), and these were compared with visual inspection performed by specialists based on the Wells criteria [21], [22]. Finally, semi-supervised clustering has been used for distinguishing patterns in AF AEGs also relying on visual inspection [23], [24]. Despite providing valuable insight on AEG clustering, the performance of these methods was based on visual inspection, and this introduces subjectivity [11].

In the present work, the AEG fractionation parameters from a commercial EAM system—CARTO (Biosense Webster, Diamond Bar, California)—were used to implement an unsupervised classification and identify clusters of AEGs with similar archetype. A set of AEG-derived markers obtained from different perspectives of the AEGs—such as information theory, spectral analysis, and nonlinear dynamics—were subsequently used in this new classification to reinterpret the CARTO criterion itself. A preliminary version of this work has been reported in [25].

II. Methods

A. Study Population and Electrophysiological Study

The population consisted of 11 patients (8 males; mean age 60.7 ± 7.3 years; history of AF 57.3 ± 37.5 months) referred to Glenfield Hospital (UK) for catheter ablation of persAF. Details of the clinical characteristics of the study subjects are provided in the *Supplementary Material*. All patients were in AF at the start of the procedure and during data collection. Study approval was obtained from the local ethics committee and all procedures were performed with full informed consent.

All antiarrhythmic drugs except amiodarone were discontinued for at least 5 half-lives before the start of the procedure. The EP study and data collection were conducted with NavX (St. Jude Medical, St. Paul, Minnesota). 3D left atrial geometry was created within NavX using a deflectable, variable loop circular PV mapping catheter (Inquiry Optima, St. Jude Medical). PVI was performed with a point-by-point wide area circumferential ablation approach (Cool Path Duo irrigated RF catheter, St. Jude Medical), followed by the creation of a single roof line ablation. PVI was defined as the abolition of electrical signals on the circular mapping catheter when positioned within each PV. Sequential point-by-point bipolar AEGs were then collected using the Inquiry and AEG fractionation maps were created to perform AEG-guided ablation. Sinus rhythm was achieved as a result of AEG-guided ablation in all cases.

B. Signal Processing

A total of 956 point-by-point bipolar AEGs were sequentially recorded from the atria (820 from the left atrium, 136 from the right atrium; 1200 Hz sampling frequency). All signals were filtered using the default filters embedded in the EAM system

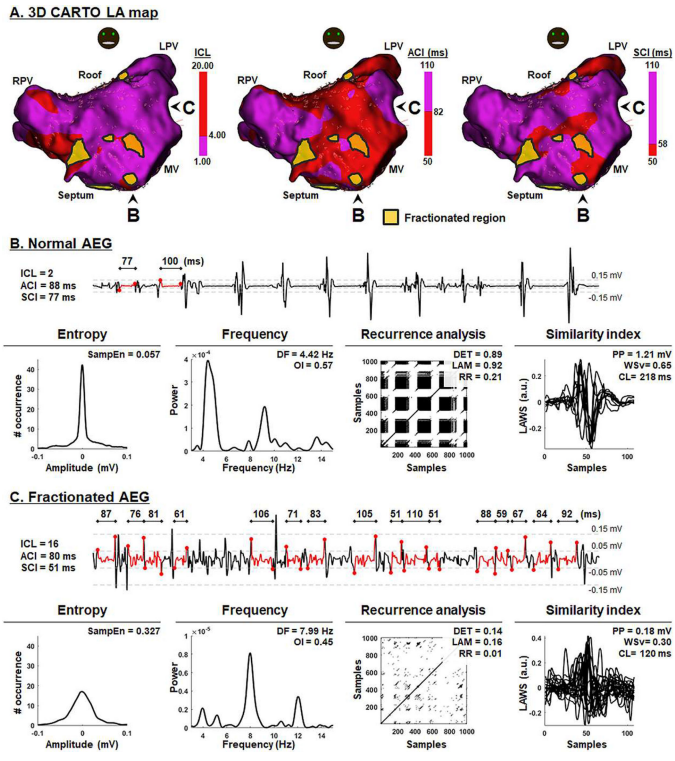

Fig. 1. (A) 3D atrial geometry in a representative patient, with superimposed automated AEG classification by CARTO algorithm. (B) Segment of a normal AEG with CARTO annotations. The nine AEG-derived markers used in the subsequent parts of the work are illustrated (further details are provided in the text). (C) Segment of a fractionated AEG with CARTO annotations. The AEG parts highlighted in red indicate the fractionated complexes annotated by CARTO. MV = mitral valve; LPV = left pulmonary veins; RPV = right pulmonary veins.

(30–300 Hz [11]) and removing power-line interference (50 Hz Notch filter). AEGs of 5 s in duration, shown to be sufficient for AEG classification [26], were used in this study. A stationary wavelet transform filter was implemented based on a previously described method to further reduce both baseline wander and high frequency noise [27]. A brief review of this method is provided in the *Supplementary Materials*.

Although the EP studies were guided by NavX, a validated offline MATLAB algorithm was used to compute the CARTO criterion. A detailed description of the methodology is provided elsewhere [11]. Briefly, CARTO provides online, automated quantification of AEG fractionation based on complex intervals between successive peaks and troughs occurring within a fixed window of sequentially recorded bipolar AEGs (Fig. 1). The number of identified complex intervals is referred to as the interval confidence level (ICL). CARTO also finds the average of the identified intervals—referred to as the average complex interval (ACI); and the shortest identified interval—referred to as the shortest complex interval (SCI). The CARTO variables (ICL, ACI and SCI) were used in the subsequent part of this study. AEGs were considered fractionated for ICL ≥ 8 (adjusted for 5 s AEGs), ACI ≤ 82 ms and SCI ≤ 58 ms [11]. This criterion was shown to counterbalance the differences of automated AEG classification performed by NavX and CARTO [11].

C. Unsupervised Classification

The k-means clustering algorithm is one of the many available methods for unsupervised classification. The algorithm aims at fragmenting an attribute space with N observations and P dimensions (variables) into a Voronoi diagram with k clusters—the k defined by the user—so that the within-cluster sum of squares is minimized. Each observation is assigned to a cluster based on the squared Euclidean distance as the measure of dissimilarity between data points and the clusters means (or centroids). At each iteration, the means of the clusters are recalculated with the newly assigned data points. This process is repeated until the within-cluster sum of squares is minimized, and no additional points are assigned to the clusters [28].

The three variables calculated by CARTO were chosen as inputs to the unsupervised classification, since they are broadly accepted and used for AF mapping in EP studies [11]. Min-Max method was used to normalize the variables between 0-1 (referred to as $\overline{\text{ICL}}$, $\overline{\text{ACI}}$ and $\overline{\text{SCI}}$) in order to avoid scaling bias (*Supplementary Materials*).

Three different methods were used for estimating the number of classes within the 3D attribute space formed by $\overline{\text{ICL}}$, $\overline{\text{ACI}}$ and $\overline{\text{SCI}}$: the elbow [29], the average silhouette [30], and the gap statistic [31]. Each method tested the number of clusters from 2 to 15. Fifty tests were performed for each number of clusters to avoid bias from initial conditions. A review on the methods for estimating the number of classes is provided in the *Supplementary Materials*.

K-means was implemented following the number of classes defined by the three above-mentioned methods. Random initialization of centroid locations was repeated 50 times to minimize bias from initial conditions and provide the solution with the lowest total sum of distances among all the replicates. K-means++ was used for cluster center initialization.

D. Attributes Used to Characterize the AEG Classes Found With the k-Means

Nine attributes measured from the AEGs used in previous studies as AF markers were selected to quantitatively characterize the AEG classes found by k-means clustering. They were grouped into four categories, as follows:

1) *Information theory attribute: Sample entropy (SampEn).* This entropy measure provides a direct estimation of the amplitude distribution of a signal and, therefore, of its complexity [32]. SampEn was reported to correlate with the core of rotors during FIRM mapping [32], which might contribute to EP studies targeting re-entries during ablation [6].
2) *Frequency-based attributes: DF and organization index (OI).* DF is the frequency of AEG spectrum peak and describes the rate of the AF activation process [10]. OI is a measure of the spectrum dispersion and is bounded between 0 and 1, with smaller values indicating more fractionated AEGs [33]. Frequency analysis helps to identify atrial regions with high activation rate (higher DF) during AF, whose ablation was suggested as an effective way to organize AF [10].

3) *Recurrence quantification analysis-based attributes: determinism (DET), laminarity (LAM) and recurrence rate (RR).* A recurrence plot (RP) is a graphical technique used to characterize phase transitions and unveil underlying nonlinear phenomena in general [34]. Recurrence quantification analysis (RQA) variables, mainly those based on diagonal and vertical (horizontal) structures of the RP, can be used for a better inference of the generative model [34]. Rigorous steps for a proper reconstruction of RPs and for the estimation of RQA attributes extracted from AF AEGs were proposed in [35].
4) *Time-domain activation wave attributes: wave similarity (WS), peak-to-peak (PP) voltage, and cycle length (CL).* These attributes are based on the extraction of local atrial activation waveforms, which provide direct information on the atrial activation process. WS is a measure of the repetitiveness of activation wave morphology in AEGs, and reflects the organization of the underlying conduction patterns [14]. PP quantifies the AEG voltage amplitude and might help to identify regions with low voltage, which are believed to correlate with the presence of fibrotic tissue [9]. CL represents the rate of activation of the underlying atrial tissue estimated in the time-domain. CL lengthening is often observed before AF termination during ablation [36], and is used as surrogate outcome in ablation procedures [14], [37].

These attributes are illustrated in Fig. 1(B) and 1(C), and a brief review is provided in the *Supplementary Materials*. All attributes were estimated from the original signals.

E. Statistical Analysis

All continuous non-normally distributed variables are expressed as median and interquartile range. Nonparametric unpaired multiple data were analyzed using the Kruskal-Wallis test with Dunn's correction, while nonparametric unpaired data were analyzed using the Mann–Whitney test. A robust multivariate analysis of variance (MANOVA) using Munzel and Brunner's method was implemented to test the AEG classes found by the k-means clustering in the 3D attribute space defined by the CARTO variables [38]. P-values of less than 0.05 were considered statistically significant.

III. Results

A. Identification of the Number of AEG Classes

Data normalization can affect the k-means clustering. Therefore, it is important that the input values for the model represent realistic ranges for the reproducibility of the method and generalization of the results. ACI and SCI are lower and upper bounded (50 – 110 ms), and both minimum and maximum values were found in the present cohort of patients. ICL is lower bounded to 1 (also found in the present work), and the highest ICL in the cohort was 33, which offers a valid representation of the EP phenomena [11].

The 3D distribution defined by the three normalized CARTO attributes ($\overline{\text{ICL}}$, $\overline{\text{ACI}}$ and $\overline{\text{SCI}}$) is shown on Fig. 2(A). 692 (72%) AEGs were classified as normal by CARTO and 264 (28%) were classified as fractionated (Fig. 2(B)). Fractionated AEGs showed significantly higher ICL, and significantly lower ACI and SCI ($P<0.0001$, Fig. 2(C)).

The tests for estimating the number of classes are illustrated in Fig. 3. The different methods used to determine the number of classes provided consistent results. The elbow method suggested a discontinuity in slope between clusters 5 and 6 (Fig. 3(A)). The average silhouette showed a high value for 2 clusters following local maxima at 5 clusters (Fig. 3(B)). Finally, the gap statistic method showed an overlap of one standard deviation between clusters 9 and 10. The differences within gap statistic, however, decreased drastically after 5 clusters, suggesting a convergence to the optimal number of clusters (Fig. 3(C)). Based on these criteria, 5 classes of AEGs were adopted in subsequent analyses.

B. Unsupervised Classification on the 3D Attribute Space Defined by CARTO Variables

Most of the AEGs classified as normal following the CARTO criterion were further divided into 4 classes by k-means clustering (classes 1 to 4), while AEGs classified as fractionated were mostly aggregated in class 5 (Fig. 4(A)). The positions of the centroids found by the k-means are highlighted in Fig. 4.

The k-means classification breakdown (in %) for each patient is shown in Fig. 4(B), while the 3D distribution space breakdown in each patient is included in the *Supplementary Materials*. Since almost all patients displayed signals from all five classes, the distributions suggest that the classification was effective in distinguishing specific regions within each patient's atria rather than distinguishing between patients.

The decision boundaries created by the k-means are highlighted in Fig. 4(C). Class 1 (43%) represented normal AEGs with the lowest ICL and highest ACI and SCI (Fig. 4(D)). Class 2 (12%) and 3 (13%) showed similar low ICL, but class 3 showed AEGs with shorter ACI when compared to class 2. Class 4 (30%) suggested moderated fractionation, with high ACI but low SCI. Class 5 (20%) presented very similar distribution compared to the AEGs classified as fractionated by CARTO. AEGs in this class showed very high ICL, low ACI and SCI. 65% of AEGs classified as fractionated by CARTO were in class 5, 32% in class 4 and 3% in class 3. MANOVA suggested a significant effect of the k-means classes on the CARTO variables ($F = 582$, $P<0.0001$).

C. Multiparametric Characterization of AEG Classes

All nine attributes—except for DF—highlighted differences when comparing normal *vs*. fractionated AEGs (Fig. 5). As expected, OI, DET, LAM, RR, WS, and CL were significantly smaller for fractionated AEGs, while SampEn and—interestingly—PP showed significantly higher values for fractionated AEGs. These differences were further detailed when analyzing the attributes within the five classes identified by the k-means (Fig.s 6 and 7).

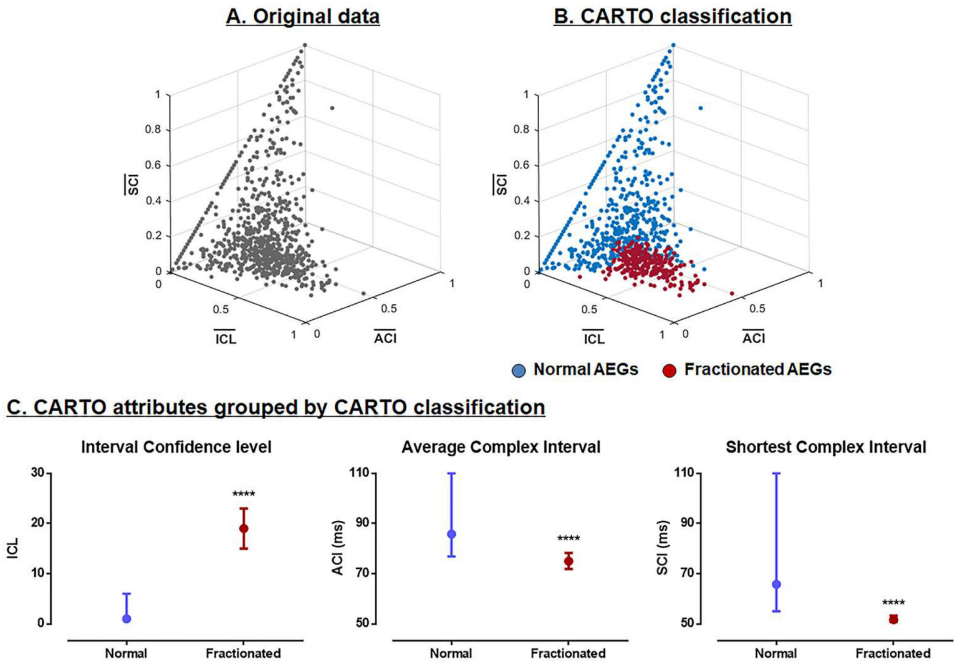

Fig. 2. 3D space distribution for all patients defined by the CARTO attributes (ICL, ACI and SCI). (A) Original space distribution prior to any classification. (B) Space distribution with the CARTO annotations for normal and fractionated AEGs. (C) CARTO attributes (ICL, ACI and SCI) grouped into normal and fractionated AEGs. Data are median and interquartile range.

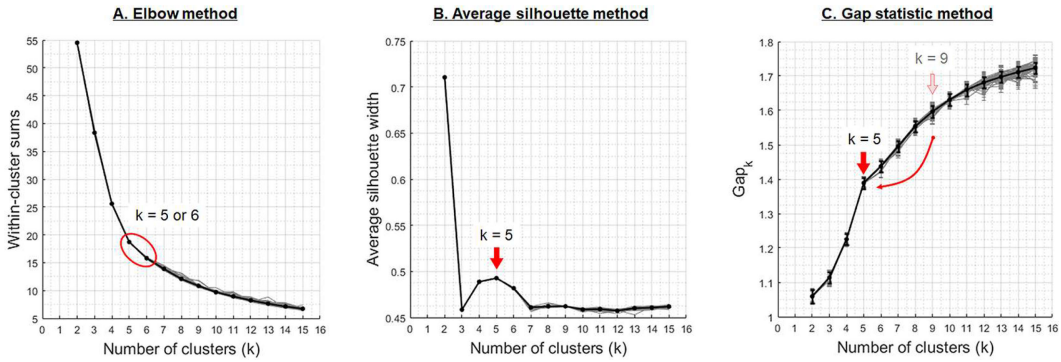

Fig. 3. Unsupervised methods for the definition of the optimal number of AEG classes. A. the elbow method identified 5 or 6 classes; B. the average silhouette method identified 5 classes; C. the gap statistic method showed an overlap of one standard deviation between 9 and 10 classes, but the differences within gap statistic decreased drastically after 5 classes.

Class 1 included AEGs with distinct and organized activations separated by electric inactivity. AEGs in this class had high OI and WS, long CL, and low SampEn, reflecting temporal and spectral organization. The high DET, LAM, and RR also suggested organized underlying dynamics. AEGs in class 1 showed low PP.

Class 2 contained AEGs with dynamic behavior similar to class 1, but with faster activation rate, resulting in high DET, LAM, and RR, but with significantly lower CL. AEGs in this class showed few occurrences of fractionated activity, resulting in lower WS and OI when compared to class 1.

In class 3, low amplitude fractionated activity was commonly observed, often intercalating with organized activation. This resulted in increased SampEn and lower OI and WS. The intercalation of low amplitude fractionated complexes and organized activity resulted in longer CL in this class.

In class 4, the organized activation deteriorated to fractionated bursts separated by isopotential lines. In consequence of such intermittent 'electric silence', the AEGs still held high DET, LAM, and RR, but now with lower SampEn, OI, and WS and shorter CL. This class already showed significantly higher values of PP.

Finally, class 5 included AEGs with continuous 'turbulent activity', with no distinguishable isopotential lines nor activations. AEGs in this class showed high SampEn and DF, and low OI, DET, LAM, RR, WS, and CL. AEGs in class 5 showed significantly higher PP.

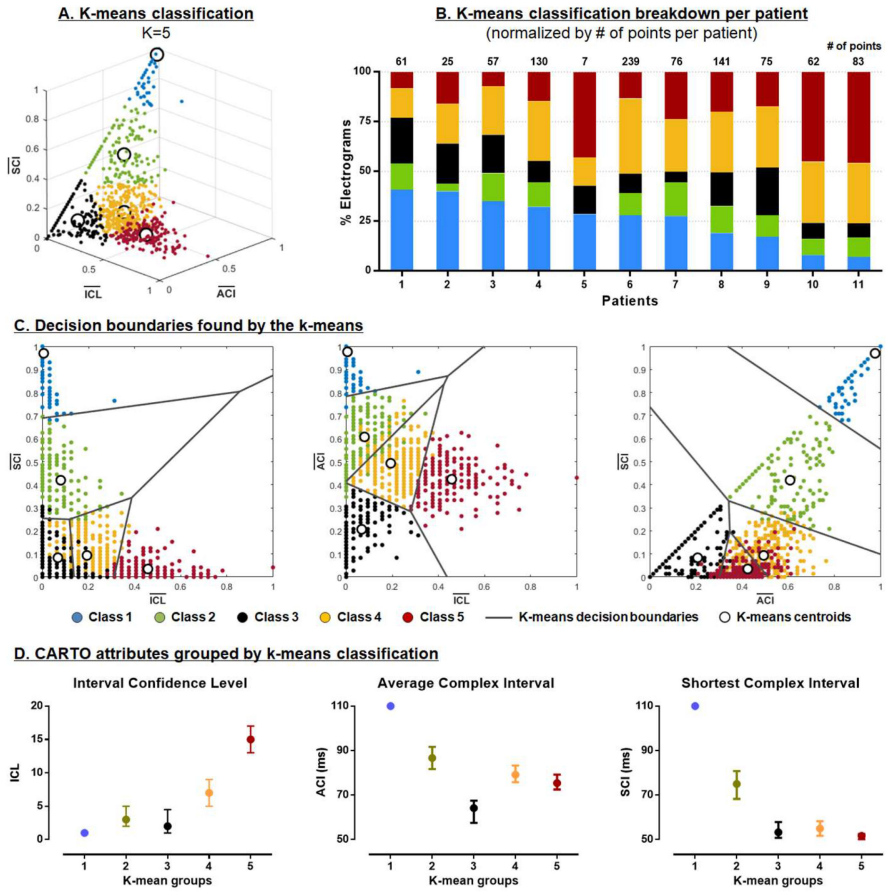

Fig. 4. A. 3D space distribution of the normalized CARTO attributes for all patients with the k-means annotations for the 5 classes from all patients. The centroids found by the k-means are highlighted as white dots in each class for $\overline{\mathrm{ICL}}$, $\overline{\mathrm{ACI}}$ and $\overline{\mathrm{SCI}}$, and are:Class 1: 0.006, 0.976, 0.970 (1.2, 108.6, 108.2); Class 2: 0.079, 0.607, 0.420 (3.5, 86.4, 75.2); Class 3: 0.067, 0.207, 0.084 (3.1, 62.4, 55.0); Class 4: 0.193, 0.493, 0.094 (7.2, 79.6, 55.6); Class 5: 0.458, 0.424, 0.035 (15.7, 75.4, 52.1).B. K-means classification breakdown (in %) for each patient. C. 2D Representations of the Voronoi diagrams and the decision boundaries delineated by the k-means projected on the planes defined by pairs of the normalized CARTO attributes (all patients). D. CARTO attributes (ICL, ACI and SCI) grouped into the 5 classes defined by k-means clustering. Data are median and interquartile range. MANOVA suggested a significant main effect of the k-means groups (1 to 5) on the CARTO attributes ($F = 582$, $P < 0.0001$). $^{****}P < 0.0001$.

IV. Discussion

In the present work, we used the variables calculated by a commercial EAM system to implement an unsupervised classification. To the best of our knowledge, this is the first work to use clustering on the three markers provided by CARTO and to perform an extensive investigation to interpret the discovered classes with possible underlying EP phenomena. Accordingly, five classes of AEGs were found from the clustering. A set of AEG-derived markers—each of which sensitive to different properties of the arrhythmia—showed that these classes denoted AEGs with distinct characteristics that could potentially represent different EP mechanisms. Thus, the proposed approach may help to reinterpret and reframe the CARTO criterion itself and may provide a more comprehensive characterization of the atrial substrate.

A. Patient-Specific Atrial Substrate in persAF

While some previous work has suggested that the ablation of additional sites beyond PVI does not improve freedom from AF [13], other recent findings support tailored ablation following PVI to target patient-specific AF drivers [39], [40]. We have shown in a recent publication that the presence of PV drivers might hinder the identification of non-PV drivers, even in regions distant from ablation lesions [8]. Atrial regions impervious to PVI may host important AF sources, which may persist after PVI driving the arrhythmia. These results, therefore, support the perception that atrial mapping—and ablation—should be performed after PVI. Consequently, the method proposed in the present work was developed using AEGs collected after PVI. Additionally, different sources of AF have been reported, and different solutions have been introduced for tailored identification [3], [6], [9], [10].

These drivers, however, are not mutually exclusive, and may therefore co-exist during persAF. As a result, when choosing one method to identify an AF driver—as it is usually the case when using an EAM system for automated AF mapping—other existing mechanisms might result undetected, and AF ablation might not target all relevant drivers necessary to terminate AF. Consequently, novel methods for AF mapping should consider

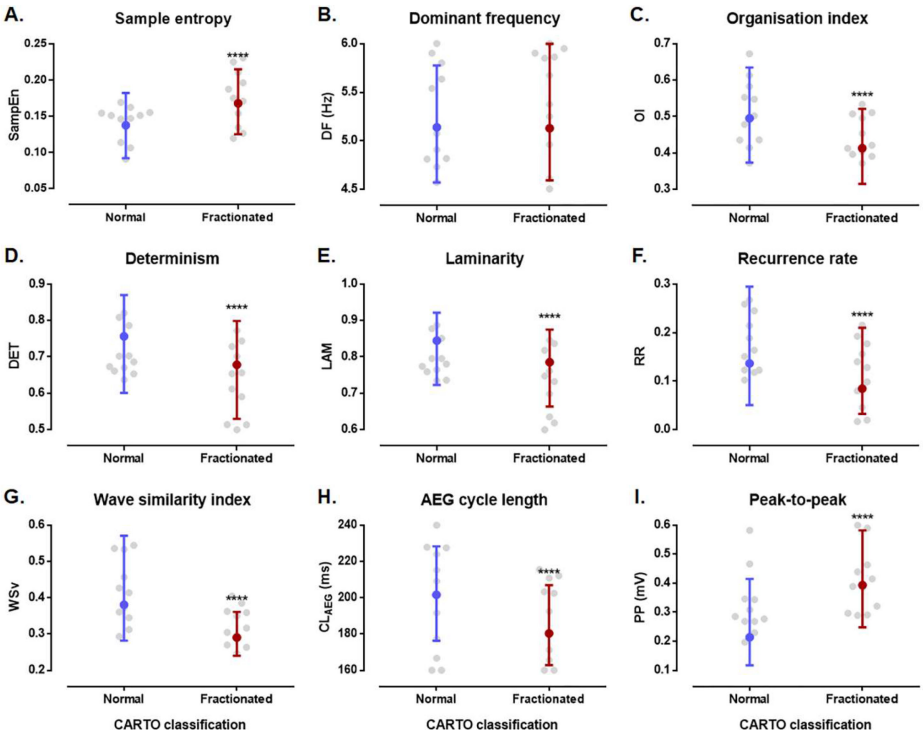

Fig. 5. The nine AEG-derived markers grouped into normal and fractionated AEGs according to the CARTO criterion. Data are median and interquartile range calculated on the AEG distributions. Patient-based mean values are superimposed in light grey. $^{****}P < 0.0001$.

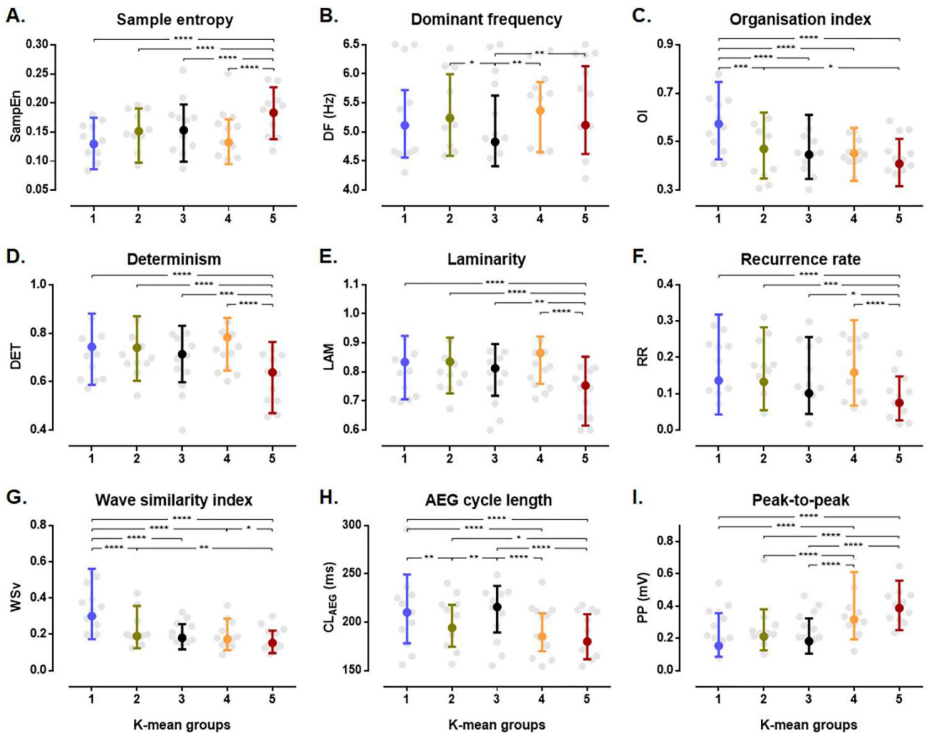

Fig. 6. The nine AEG-derived markers grouped into the five AEG classes found by the k-means. Data are median and interquartile range calculated on the AEG distributions. Patient-based mean values are superimposed in light grey. $^{****}P < 0.0001$; $^{***}P < 0.001$; $^{**}P < 0.01$; $^{*}P < 0.05$.

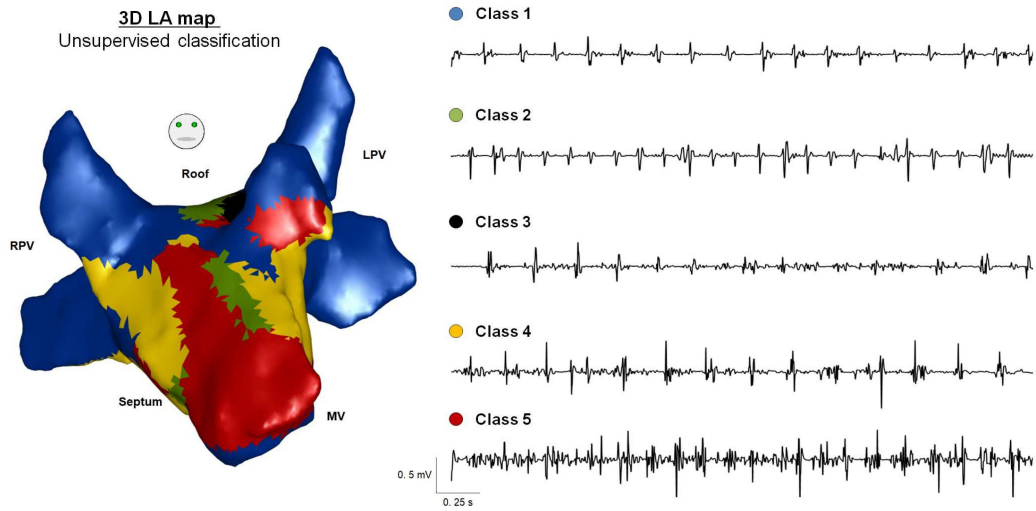

Fig. 7. Representative 3D atrial map color-coded with the unsupervised classification and samples of AEGs from each class found by k-means clustering. Details about each class of AEGs are provided in the text.

the multifaceted aspects of AEGs by extracting attributes that explain different EP characteristics of the underlying atrial tissue. The proposed framework of clustering and subsequent AEG classification provide a more detailed characterization of the atrial substrate that may be easily translated to this novel setting.

B. PersAF AEG Classification

Classification based on AEG visual inspection performed by specialists during EP studies became widely used to characterize the atrial substrate [22]. It was adopted as the 'gold reference' for many years, and many works relied on it in the investigation of methods for substrate characterization [41]. Despite the valuable contribution of those investigations, the visual assessment of AEGs introduces subjectivity to the method and depends on user's experience. Additionally, the visual inspection might not correspond to the true atrial substrate. These factors may produce inconsistencies and can hinder the reproducibility of AEG classification [11].

So far, ablation targeting atrial regions automatically identified by commercial systems has failed to provide a definitive solution for persAF therapy [12], [13]. In addition, most EP studies consider only one attribute calculated by such systems to characterize the atrial tissue and guide ablation based on a dichotomous criterion—to ablate or not to ablate [11].

Therefore, not only we do not know what is driving the arrhythmia, but we also do not know whether the binary classification performed by current methods suffices.

The five AEG classes found in the present work corroborate and expand the four classes initially proposed by Wells and colleagues [22]. These five classes were obtained by combining CARTO variables (ICL, ACI and SCI), which were initially proposed for an automatic classification of signals into two classes (*i.e.*, normal versus fractionated AEGs). While the combination of the three variables calculated by CARTO might seem redundant—or as different formulations of similar rules—the motivation of the work was to investigate possible limitations of the dichotomous criteria applied by such systems in the characterization of the atrial substrate during persAF without performing visual inspection of AEGs. Considering this lack of 'ground truth', unsupervised classification was used to investigate possible classes of AEGs.

Similar to our results, five classes of atrial signals were found during AF in a previous work using the average silhouette [20]. Although this result was obtained using 12-lead ECG recordings instead of intracardiac measurements, this highlights the—yet not fully understood—underlying complexity of this arrhythmia. Despite great debate, the definition of types of AF is often subjective, and not necessarily based on EP characteristics [42]. For instance, AF is usually defined as paroxysmal, persistent, long-term persistent or permanent [1]. This is based on the arrhythmia history, self-termination and termination followed by external interference (*e.g.*, cardioversion). Although it can be challenging to compare the five classes of atrial signals found in the present work (intracardiac) and those found from the ECGs, the results from unsupervised classification help to expand the traditional classifications in both cases, paving novel ways to the investigation of the complex EP phenomena driving this arrhythmia, its diagnostic and its therapy.

Unsupervised classification has been also applied to intracardiac recordings. Different classes of activations were identified within single AF AEGs with PCA—between 3 and 20 [21]. Such heterogeneity of atrial activations intra-AEGs supports the different characteristics and complexities found in the five classes of AEGs in our work. Semi-supervised clustering was investigated for distinguishing patterns in AF AEGs [23], [24]. However, the number of classes in those works was defined based on the four different types of AEGs identified by visual inspection according to Wells' criteria [22], tailoring the output classification [11].

C. Multivariate AEG Characterization

Sustained AF causes changes in the cardiac tissue characteristics, inducing structural and electric remodeling [1]. These regions can potentially host sources of AF, which are characterized by different mechanisms. For instance, structural changes represented by fibrotic tissue could induce slow or inhomogeneous conduction, which might result in re-entry circuits and fractionated fibrillatory conduction [3]. Such turbulent activity, in turn, might induce multiple wavelets to meander in the cardiac tissue, creating a self-sustaining arrhythmogenic mechanism [4]. Similarly, electric remodeling can result in rapidly discharging automatic foci [2], creating regions with ectopic beats that drive the arrhythmia. More importantly, these changes are specific to each patient, and they might co-exist, either simultaneously or intermittently. Hence, tailored ablation strategies are needed to guide ablation considering the persAF pathophysiology found in each patient, even in the presence of multiple sources for AF.

In the present work, a variety of markers—measuring peculiar AEG characteristics—was used to characterize the five classes found by the unsupervised classification. Since the rhythmic and morphological properties of AEGs reflect the underlying atrial propagation patterns and substrates [14], [43], the five classes might be associated with distinct arrhythmogenic mechanisms. For instance, AEGs collected from healthy cardiac tissues are usually described by organized activations separated by electric inactivity, temporal and spectral organization and organized underlying dynamics. Such characteristics reflect homogeneous and organized underlying cardiac activation wavefronts. Additionally, it should be expected that these features would result in high OI and WS, long CL, and low SampEn, as well as high DET, LAM, and RR. All the above were found in class 1 AEGs, which suggests that AEGs in this class represent healthy cardiac tissue. Interestingly, we have recently shown that AEGs with relatively low DF and high OI correlate with atrial regions that terminated AF following local ablation [44]. The AEGs found in class 1 of the present study also showed slow rate and high OI suggesting that these AEGs could represent targets for ablation depending on the strategy defined [45].

Conversely, class 2 AEGs were similar to AEGs in class 1, but with significantly faster activation rates. Consequently, AEGs found in this class have shown high DET, LAM and RR, but with significantly lower CL. Such AEGs could correlate with regions presenting ectopic beats, breakthroughs due to endo-epicardial dissociation, and/or reentries [6], [7], [10].

Class 3 represents AEGs with deteriorated temporal behavior in which organized activation intercalates with fractionated activity. Such unstable dynamics resulted in increased SampEn and lower OI and WS. This unstable dynamics are suggestive of a passive phenomenon in which organized wavefronts alternate with turbulent, multi-wavelet propagation [26]. The fractionated activity becomes more evident in AEGs from class 4, with fractionated bursts separated by isopotential lines, resulting in low SampEn, OI, and WS and shorter CL. This might represent atrial regions with remodeled substrate, unable to sustain the high frequency activation from organized wavefronts [3].

Finally, AEGs in class 5 have shown continuous 'turbulent activity', with no distinguishable isopotential lines nor activations, which was reflected in high SampEn and DF, and low OI, DET, LAM, RR, WS and CL. These regions may correspond to remodeled tissue with high degree of fibrosis. Interestingly, AEGs in this class showed significantly higher PP, which is counterintuitive given that previous work has suggested that low-voltage areas in the atria correlate with fibrotic regions that would actively participate in AF perpetuation [9]. Nevertheless, further studies are needed to consolidate these results given that bipolar voltage values may be affected from a variety of confounding factors [46], [47].

Our results offer a novel avenue of research to correlate these classes of persAF AEGs with underlying EP mechanisms and explore their clinical efficacy. For instance, when ablation is addressed to fast pacing regions—which could correlate with ectopic beats, transmural conduction or rotors [6], [7], [10]—AEGs in class 2 may be targeted during ablation. On the other hand, in the case of targeting regions with turbulent activations—which could correlate with fibrotic tissue, anisotropic conduction and also rotors [3], [9]—AEGs in classes 4 and/or 5 may be targeted during ablation.

D. Limitations and Future Perspectives

The present study represents an additional step in our understanding of the underlying AF pathophysiology through the investigation of bipolar AEGs. Although the use of features from an EAM system may allow quicker and wider clinical application of our method, further investigations are still needed before any prospective clinical study is performed. Standardized thresholds for the classifications must be refined based on larger populations, although a likely generalization of unsupervised classification is suggested by the single patient k-means in Fig. 4(B). In addition, the proposed unsupervised clustering framework may be extended to other attributes to better highlight possible different classes of AEGs in persAF.

K-means may not be suited for all types of data and it may underperform in the presence of outliers and in non-globular clusters. While k-means was chosen for its simplicity in this attempt to investigate possible sub-groups of AEGs, other methods should be investigated in future works.

The current study was limited to retrospective, point-by-point sequentially collected data, making it challenging to infer on the EP mechanisms underlying each AEG class. Further investigations would be helpful for the validation of the suggested method, such as with biophysical computational models to reproduce atrial activity and ablation procedures [48].

V. Conclusion

The present work provides a more detailed atrial substrate characterization based on an unsupervised classification of persAF AEGs. Variables calculated by a commercial EAM system broadly used in EP studies—CARTO—were used to create a 3D attribute space. The optimal number of classes of AEGs were found by three different clustering methods (elbow, average

silhouette, and gap statistic). K-means clustering was used to further investigate those five AEG classes. Each class showed distinct characteristics that could be related to different EP mechanisms according to nine AEG-derived markers.

Our results reinterpret the classes of AEGs usually found in persAF in the absence of a ground truth, expanding the traditional dichotomous AEG classification proposed by commercial EAM systems without relying on the subjectivity of visual inspection while providing a more complete representation of the underlying EP phenomena. We introduced operative rules that can help defining the ablation strategy based on EP characteristics reflected on the AEG classes, which could provide a more complete characterization of persAF substrate during ablation target identification in future clinical studies.

Acknowledgment

The authors thank Zakariyya Vali, Karina Almeida, Luciana Mizioka, Henrique Pereira and members of the Institute of Biotechnology (IBT) from the Karlsruhe Institute of Technology (KIT) for the productive discussions. FSS is grateful to a Study Leave from the University of Leicester.

References

[1] H. Calkins *et al.*, "2017 HRS/EHRA/ECAS/APHRS/SOLAECE expert consensus statement on catheter and surgical ablation of atrial fibrillation," *Heart Rhythm*, vol. 14, pp. e275–e444, Oct. 2017.

[2] M. Haissaguerre *et al.*, "Spontaneous initiation of atrial fibrillation by ectopic beats originating in the pulmonary veins," *N. Engl and J. Med.*, vol. 339, pp. 659–66, Sep. 3, 1998.

[3] K. Nademanee *et al.*, "A new approach for catheter ablation of atrial fibrillation: Mapping of the electrophysiologic substrate," *J. Amer. College Cardiol.*, vol. 43, pp. 2044–2053, 2004.

[4] K. T. Konings *et al.*, "High-density mapping of electrically induced atrial fibrillation in humans," *Circulation*, vol. 89, pp. 1665–1680, Apr. 1994.

[5] J. Jalife, O. Berenfeld, and M. Mansour, "Mother rotors and fibrillatory conduction: A mechanism of atrial fibrillation," *Cardiovascular Res.*, vol. 54, pp. 204–216, May 2002.

[6] S. M. Narayan *et al.*, "Treatment of atrial fibrillation by the ablation of localized sources: CONFIRM (Conventional Ablation for Atrial Fibrillation With or Without Focal Impulse and Rotor Modulation) trial," *J. Amer. College Cardiol.*, vol. 60, pp. 628–636, Aug. 14, 2012.

[7] N. de Groot *et al.*, "Direct proof of endo-epicardial asynchrony of the atrial wall during atrial fibrillation in humans," *Circ. Arrhythm. Electrophysiol.*, vol. 9, May 2016.

[8] T. P. Almeida *et al.*, "Atrial electrogram fractionation distribution before and after pulmonary vein isolation in human persistent atrial fibrillation—A retrospective multivariate statistical analysis," *Frontiers Physiol.*, vol. 8, 2017.

[9] A. Boldt *et al.*, "Fibrosis in left atrial tissue of patients with atrial fibrillation with and without underlying mitral valve disease," *Heart*, vol. 90, pp. 400–405, Apr. 2004.

[10] F. Atienza *et al.*, "Real-time dominant frequency mapping and ablation of dominant frequency sites in atrial fibrillation with left-to-right frequency gradients predicts long-term maintenance of sinus rhythm," *Heart Rhythm*, vol. 6, pp. 33–40, Jan. 2009.

[11] T. P. Almeida *et al.*, "Minimizing discordances in automated classification of fractionated electrograms in human persistent atrial fibrillation," *Med. Biol. Eng. Comput.*, vol. 54, pp. 1695–1706, Nov. 2016.

[12] E. Buch *et al.*, "Long-term clinical outcomes of focal impulse and rotor modulation for treatment of atrial fibrillation: A multicenter experience," *Heart Rhythm*, vol. 13, pp. 636–641, Mar. 2016.

[13] A. Verma *et al.*, "Approaches to catheter ablation for persistent atrial fibrillation," *New Engl. and J. Med.*, vol. 372, pp. 1812–1822, May 7, 2015.

[14] F. Ravelli and M. Masè, "Computational mapping in atrial fibrillation: How the integration of signal-derived maps may guide the localization of critical sources," *EP Europace*, vol. 16, pp. 714–723, 2014.

[15] C. M. Bishop, *Pattern Recognition and Machine Learning*. Berlin, Germany: Springer, 2006.

[16] A. K. Feeny *et al.*, "Artificial intelligence and machine learning in arrhythmias and cardiac electrophysiol," *Circulation: Arrhythmia Electrophysiology*, 2020.

[17] C. Wen *et al.*, "Classification of ECG complexes using self-organizing CMAC," *Measurement*, vol. 42, pp. 399–407, 2009.

[18] F. Sufi and I. Khalil, "Diagnosis of cardiovascular abnormalities from compressed ECG: A data mining-based approach," *IEEE Trans. Inf. Technol. Biomed*, vol. 15, no. 1, pp. 33–39, Jan. 2011.

[19] Y.-C. Yeh, C. W. Chiou, and H.-J. Lin, "Analyzing ECG for cardiac arrhythmia using cluster analysis," *Expert Syst. Appl.*, vol. 39, pp. 1000–1010, 2012.

[20] F. I. Donoso *et al.*, "Clustering of atrial fibrillation based on surface ECG measurements," in *Proc. Conf. Proc. IEEE Eng. Med. Biol. Soc.*, 2013, vol. 2013, pp. 4203–4206.

[21] L. Faes *et al.*, "Principal component analysis and cluster analysis for measuring the local organisation of human atrial fibrillation," *Med. Biol. Eng. Comput.*, vol. 39, pp. 656–663, Nov. 2001.

[22] J. L. Wells *et al.*, "Characterization of atrial-fibrillation in man - studies following open-heart surgery," *Pace-Pacing Clin. Electrophysiol.*, vol. 1, pp. 426–438, 1978.

[23] A. Orozco-Duque, J. Bustamante, and G. Castellanos-Dominguez, "Semi-supervised clustering of fractionated electrograms for electroanatomical atrial mapping," *Biomed. Eng. Online*, vol. 15, Apr. 26, 2016.

[24] A. Orozco-Duque *et al.*, "Electroanatomical mapping based on discrimination of electrograms clusters for localization of critical sites in atrial fibrillation," *Prog. Biophys. Mol. Biol.*, vol. 141, pp. 37–46, Jan. 2019.

[25] T. P. Almeida *et al.*, "Unsupervised k-mean classification of atrial electrograms from human persistent atrial fibrillation," in *Proc. Comput. Cardiol. Conf.*, 2018, pp. 1–4.

[26] T. P. Almeida *et al.*, "The temporal behavior and consistency of bipolar atrial electrograms in human persistent atrial fibrillation," *Med. Biol. Eng. Comput.*, vol. 56, pp. 71–83, Jan. 2018.

[27] C. Schilling, "*Analysis of Atrial Electrograms," PhD, Elektrotechnik und Informationstechnik des Karlsruher Instituts für Technologie, Karlsruhe Institute of Technology*, KIT Scientific Publishing, 2012.

[28] J. MacQueen, "Some methods for classification and analysis of multivariate observations," in *Proc. 5th Berkeley Symp. Math. Statist. Probability*, 1967, vol. 1, pp. 281–297.

[29] R. L. Thorndike, "Who belongs in the family?" *Psychometrika*, vol. 18, pp. 267–276, Dec. 01, 1953.

[30] P. J. Rousseeuw, "Silhouettes: A graphical aid to the interpretation and validation of cluster analysis," *J. Comput. Appl. Math.*, vol. 20, pp. 53–65, 1987.

[31] R. Tibshirani, G. Walther, and T. Hastie, "Estimating the number of clusters in a data set via the gap statistic," *J. Royal Statist. Soc.: Ser. B (Statist. Methodol.)*, vol. 63, pp. 411–423, 2001.

[32] A. N. Ganesan *et al.*, "Bipolar electrogram shannon entropy at sites of rotational activation: Implications for ablation of atrial fibrillation," *Circ Arrhythm Electrophysiol.*, vol. 6, pp. 48–57, Feb. 2013.

[33] T. H. T. Everett *et al.*, "Assessment of global atrial fibrillation organization to optimize timing of atrial defibrillation," *Circulation*, vol. 103, pp. 2857–2861, Jun. 12, 2001.

[34] N. Marwan *et al.*, "Recurrence plots for the analysis of complex systems," *Phys. Rep.*, vol. 438, pp. 237–329, 2007.

[35] T. P. Almeida *et al.*, "Characterization of human persistent atrial fibrillation electrograms using recurrence quantification analysis," *Chaos*, vol. 28, pp. 085710-1–085710-12, 2018.

[36] I. B. Kim *et al.*, "Relationship between local atrial fibrillation interval and refractory period in the isolated canine atrium," *Circulation*, vol. 94, pp. 2961–2967, Dec. 1, 1996.

[37] F. Ravelli *et al.*, "The logical operator map identifies novel candidate markers for critical sites in patients with atrial fibrillation," *Prog. Biophys. Mol. Biol.*, vol. 115, pp. 186–197, Aug. 2014.

[38] U. Munzel and E. Brunner, "Nonparametric tests in the unbalanced multivariate one-way design," *Biometrical J.*, vol. 42, pp. 837–854, 2000.

[39] M. Ohe *et al.*, "New tailored approach using a revised assessment of fragmented potentials for persistent atrial fibrillation: Early area defragmentation by modified CFAE module," *J. Cardiovascular Electrophysiol.*, vol. 30, pp. 844–853, 2019.

[40] P. Henley *et al.*, "Single-center experience of the FIRM technique to ablate paroxysmal and persistent atrial fibrillation," *J. Cardiovascular Electrophysiol.*, vol. 30, pp. 493–502, Apr. 2019.

[41] C. D. Cantwell *et al.*, "Rethinking multiscale cardiac electrophysiology with machine learning and predictive modelling," *Comput. Biol. Med.*, vol. 104, pp. 339–351, Jan. 2019.

[42] J. G. Andrade *et al.*, "Association of atrial fibrillation episode duration with arrhythmia recurrence following ablation: A secondary analysis of a randomized clinical trial," *JAMA Netw. Open*, vol. 3, Jul. 1, 2020, Paper e208748.

[43] K. T. S. Konings *et al.*, "Configuration of unipolar atrial electrograms during electrically induced atrial fibrillation in humans," *Circulation*, vol. 95, pp. 1231–1241, Mar. 4, 1997.

[44] X. Li *et al.*, "A k-nearest neighbours classifier for predicting catheter ablation responses using noncontact electrograms during persistent atrial fibrillation," in *Proc. Comput. Cardiol. Conf.*, 2018, pp. 1–4.

[45] S. Honarbakhsh *et al.*, "Drivers in AF colocate to sites of electrogram organization and rapidity: Potential synergy between spectral analysis and STAR mapping approaches in prioritizing drivers for ablation," *J. Cardiovascular Electrophysiol.*, vol. 31, pp. 1340–1349, Jun. 2020.

[46] E. Anter and M. E. Josephson, "Bipolar voltage amplitude: What does it really mean?" *Heart Rhythm*, vol. 13, pp. 326–327, Jan. 2016.

[47] T. Yamaguchi, A. Fukui, and K. Node, "Bipolar voltage mapping for the evaluation of atrial substrate: Can we overcome the challenge of directionality?" *J. Atr. Fibrillation*, vol. 11, Feb./Mar. 2019, Art. no. 2116.

[48] M. W. Krueger *et al.*, "Towards personalized clinical in-silico modeling of atrial anatomy and electrophysiology," *Med. Biol. Eng. Comput.*, vol. 51, pp. 1251–1260, Nov. 2013.